fluids

MDPI

Article

Thermohydraulic Performance of Chevron Pin-Fins

Mohamad Ziad Saghir * and Ibrahim Ghalayini

Department of Mechanical and Industrial Engineering, Toronto Metropolitan University, Toronto, ON M5B 2K3, Canada; ighalayini@ryerson.ca
* Correspondence: zsaghir@ryerson.ca

Abstract: The present study focuses on the optimum design effectiveness in heat removal for small surfaces. Pin-fin made of solid and porous cylindrical shape forming chevron is investigated numerically using the finite element method. The design consists of 3-chevron and 5-chevron configurations connected to a heated block with fluid circulating between the chevron and above them. Variable Reynolds number and pin-fins height ranging from 2 mm to 8 mm are investigated. The full Navier–Stokes equation combined with the energy equation was solved in the presence of the solid pin-fins. The Darcy–Brinkman model with the effective energy equation is used in the presence of the porous pin-fins. The system is solved for Reynolds numbers ranging from 50 to 1000, thus remaining in the laminar regime. Results revealed that the best performance evaluation criterion is higher for the 8 mm porous pin-fins regardless of their permeability. If one ignores the pressure drop and friction contribution, a solid pin-fin having a height of 4 mm showed the best heat absorption mechanism.

Keywords: pin-fins; porous material; heat enhancement; performance evaluation criterion

Citation: Saghir, M.Z.; Ghalayini, I. Thermohydraulic Performance of Chevron Pin-Fins. *Fluids* **2022**, *7*, 195. https://doi.org/10.3390/fluids7060195

Academic Editors: Andrew S. Rees and Mathieu Sellier

Received: 17 May 2022
Accepted: 6 June 2022
Published: 8 June 2022

1. Introduction

One of the essential topics in engineering is saving energy. Nowadays, a mechanism to enhance heat removal and energy storage is a critical research topic. The implementation of pin-fins has improved heat removal and reduced the system's pressure drop. Martin [1] demonstrated a theoretical approach to predict the performance of chevron-type plate heat exchangers. The furrows of the sinusoidal patterns and the inclination angles of the crests have been proven to be the most vital design parameters concerning fluid friction and heat transfer. Two kinds of flow may exist between the gap between the plates. The first flow involves crossing small sub-streams following the furrows of the first and second plates. This becomes more dominant at lower inclination angles, leading to lower pressure drops. The second flow involves wavy longitudinal flow between two vertical rows of contact points; contrary to the first flow, this prevails at higher inclination angles, resulting in higher pressure drops. The combined effects of the flows are taken to derive an equation for the friction factor as a function of the inclination angle and Reynolds number. This is known as the Lévêque equation, which is utilized for modeling and developing thermal boundary layers in a fully developed laminar or turbulent flow. Applying the Lévêque equation in this study has shown a good agreement in predicting heat transfer coefficients.

Dović et al. [2] utilized a mathematical model to study the thermal and hydraulic characteristics of a chevron plate heat exchanger with inclination angles of $\beta = 28^\circ$ and $\beta = 65^\circ$. Here, the Reynolds number was in the range of $0.1 < Re < 250$. Values of $Nu/Pr^{1/3}(\mu/\mu_w)^{0.14}$, which was derived from the Lévêque equation, agree within ±13% of the measured work for channels with inclination angles of $\beta = 28^\circ$ and $\beta = 65^\circ$ at $50 < Re < 1400$. The results concur with previous literature within discrepancies of ±(15–35)%. The experiment revealed a sudden decrease of the Nu for $Re < 30$ for a plate with $\beta = 65^\circ$. Since the friction factor remains higher than the channel with $\beta = 28^\circ$, it favors the use of plates with lower inclination angles for low Re applications.

The thermal performance and pressure drop were investigated experimentally for Al_2O_3-water and MWCNT-water nanofluids in a plate heat exchanger with chevrons at an angle of 60° by Huang et al. [3]. The results were compared to plain water. The results showed that nanofluids' heat enhancement was superior to that of water at constant Reynolds numbers, but little change was observed at constant flow velocity. MWCNT-water had more intensive heat transfer deterioration when compared to Al_2O_3-water due to higher viscosity. The pressure drop was found to augment with increasing nanoparticle concentrations; however, at low nanoparticle concentrations, the pressure drop of the nanofluids was similar to plain water. The dimensionless parameter $Nu/Pr^{0.3}$ was found to be higher with nanofluids when compared to water. However, as the nanoparticle volume concentrations increased, the $Nu/Pr^{0.3}$ decreased. Overall, the heat transfer correlation agreed well with experimental data.

Al-Neama et al. [4] studied the hydrodynamic and thermal effects of chevron fins in serpentine channels within a heat exchanger. The continuous plate was broken into nine small fins with angles of 30°. The experimental and numerical results demonstrated that the total thermal resistance decreased tediously with the water flow rate. Increasing the Reynolds number increased the pressure drop and the average Nusselt number. This is due to the thermal boundary layer thickness decreasing with higher fluid velocity. The effects of various chevron angles were investigated; as the chevron angle decreased, the total thermal resistance and heat transfer increased.

Contrary to this, as the chevron angle increased, the pressure drop was found to decrease; this is caused by a more significant gap in the secondary microchannel. The friction factor of a plate heat exchanger was computed on CFD simulations using the LES technique by Zhu et al. [5]. The flow of the working fluid ranged from $10 < Re < 6000$, and the inclination angles of the chevrons were 18°, 30°, 38°, 45°, 52°, 60°, and 72°. The objective was to map the relationships between the friction factor, Reynolds numbers, and inclination angles. A friction factor diagram was developed; the friction factor results and the inclination angle over the range of Re resembled the Moody diagram. The inclination angle was analyzed as a roughness element, thus depicting larger inclination angles leading to rougher surfaces. Hence, higher friction factors were observed.

Fernandes et al. [6] studied a fluid's fully developed laminar flow in a double-sine chevron plate heat exchanger. Utilizing the POLYFLOW CFD software, the objective was to model the relationships between the tortuosity and Kozeny's coefficients with the geometric properties of the plate heat exchanger passages. The chevron/corrugation angles of interest were 29.0°, 39.8°, 48.0°, 59.0°, 74.5°, and 84.9°. The plate heat exchanger's channel aspect ratio and corrugation angles defined the tortuosity coefficient, shape factor, and coefficient pertaining to the *fRe* relationships. The tortuosity and the permeability coefficients from the friction factor relationships increased with higher channel aspect ratios and lower chevron angles. The passages of the plate heat exchanger were found to increase with lower chevron angles but experienced little influence from the channel aspect ratio.

The hydrodynamic properties and flow distributions of a plate heat exchanger with two cross-corrugated channels were investigated numerically by Tsai et al. [7]. The inclination angle was 60°, and the chevron plates were brazed together at an angle of 180°, one on top of the other. The working fluid was water, where the Reynolds numbers ranged from 170 to 1700. The friction factor of the two channels was found to have different trends when comparing numerical to experimental results. There was approximately a 20% deviation when comparing the experimental and numerical pressure drops; this is caused by secondary flows being introduced in the secondary corrugated channels due to complex geometry that was not accounted for by the κ-ε model.

Han et al. [8] simulated the three-dimensional temperature, velocity, and pressure of a chevron corrugated plate heat exchanger. The κ-ε NRG model was adopted to simulate the hydrodynamic characteristics. Based on the results, the temperature field was found to be very small in the inlet and outlet port positions, while the pressure field was found to decrease along the flow direction. From the velocity field, it was found that no matter

whether the fluid inflows or outflows from the ports, there is always a dead-zone corrugated from the side of the port resulting in a low flow rate, causing the inlet temperature to be maintained. Overall, the CFD results were in good agreement with the experimental results.

Kumar et al. [9] studied the effects of geometrical parameters on the hydraulic and thermal performance of a U-type plate heat exchanger. The plate heat exchanger consisted of two symmetrical plates with chevron angles of 60°/60° and 30°/30°, and one unsymmetrical plate with an angle of 60°/30°. The working fluid is water with Reynolds numbers ranging from 800 to 2300. The objective was to experimentally investigate the relationships between the chevron angle on the mean pressure drop, meaning friction factor, and effectiveness. Higher Reynolds numbers resulted in the momentum overcoming viscous forces. Hence, the viscosity gradient decreased. Additionally, there was less contact of fluid molecules at higher channel velocities, resulting in the friction factor decreasing. Higher chevron angles promoted inner swirling in the inter-plate channels causing the friction factor to rise. The flow maldistribution parameter increased with higher flow rates but decreased with greater chevron angles; this is associated with the variation of overall friction factor resistance, which decreases at higher mass flow rates. Pressure drops were found to increase for higher Reynolds numbers and chevron angles due to higher interferences. Overall, as the chevron angle increased, there was a positive impact on the effectiveness of plate heat exchangers. This is justified by a more significant obstruction in fluid flow, which promotes more turbulence.

The hydraulic performance of a chevron U-type plate heat exchanger was studied analytically for different aspect ratios, Reynolds numbers (200–5800), maldistribution parameters, number of channels, and port sizes by Kumar and Singh [10]; the working fluid was water. Overall, the analytical results agreed with the experimental results with a ±10% deviation. The friction factor increased with higher Reynolds numbers and with a more significant number of channels. Due to higher maldistribution, the total pressure drop increased with higher mass flow rates, aspect ratios, Reynolds numbers, and more channels. Here, the pressure drop is a function of the number of channels. The flow maldistribution parameter was found to increase when the number of channels increased. However, increasing the aspect ratio decreased the maldistribution parameter since it is a strong function of the hydraulic diameter, the number of channels, and channel velocity. Lastly, the channel velocity increased with larger port diameters due to a significant influence of port diameters on plate heat exchangers.

Naik and Matawala [11] experimented with the heat transfer of an oil-to-water fluid in a plate heat exchanger. The effects of chevron angles (30°, 45° & 60°) along with other geometric characteristics were investigated to determine their impacts on the heat transfer coefficient. Here, the Reynolds numbers ranged from 50 to 1000, and the Prandtl numbers ranged from 3 to 75. The results depict that as the mass flow rate increases for both oil and water, so does the heat transfer coefficient. Furthermore, increasing the flow rate of water decreased the outlet temperature of the oil; this increase in heat transfer is due to more cooling water being available at higher flow rates. The chevron angle of 60° was found to have the highest heat transfer coefficient. Lastly, increasing the Reynolds number was found to lower the friction factor.

Jain et al. [12] employed the κ-ε turbulence viscous model for the heat transfer and fluid flow of water in a plate heat exchanger with chevrons at 60° angles. The Reynolds numbers ranged from 400 to 1300, and the Prandtl numbers ranged from 4.4 to 6.3. The results of the numerical study were compared to experimental findings from previous literature. It was found that the experimental friction factors and Nusselt numbers were underpredicted by 2.5–14.5% and 3–18%, respectively. An explanation for this is the exclusion of the port and flow distribution areas in the numerical modeling. Lastly, the velocity vectors were found to inhibit a zig-zag pattern, and the fluid flow is mainly along the main flow direction.

Muley and Mangllik [13] experimented with a single-phase U-type plate heat exchanger with chevrons to study water's isothermal pressure drop and heat transfer. The

Reynolds and Prandtl numbers ranged from 600 to 10^4 and from 2 to 6, respectively. There are three different types of chevron plate arrangements—30°/30°, 60°/60°, and 30°/60°. The Nusselt number was found to augment with higher chevron angles; this trend is reflected in the intense swirl flow generated by greater chevron angles present in the plates. A higher friction factor was enticed despite the more significant heat transfer coefficients associated with chevrons. The friction factors were 13–44 times greater than flat plate channels due to greater flow friction in the interpolate channel. In addition to the chevron angle, the area enlargement factor influenced the hydrodynamic and thermal characteristics. Higher heat transfer rates and pressure drops were obtained with higher enlargement areas. This is expected as greater swirl mixing is promoted.

The experimental Nu and isothermal data of f were determined for cooling vegetable oil in a single-plate heat exchanger by Muley et al. [14]. The Prandtl and Reynolds numbers were in the range of $130 < Pr < 290$ and $2 < Re < 400$. Three configurations were utilized for the chevron plate arrangements: two symmetrical 30°/30° and 60°/60° plates, and one mixed plate arrangement consisting of 30°/60°. The thermohydraulic performance was heavily influenced by the chevron angle, corrugation aspect ratio, and fluid flow parameters. Under the same flow conditions, the Nusselt number was enhanced up to 3 times in the presence of chevrons compared to the equivalent flat-plate pack, while the friction factor increased 6.6 times. Lastly, depending on the Reynolds number and chevron angle, under fixed surface geometry and pumping power, the heat transfer was enhanced up to 2.9 times more than its flat-plate channels' counterpart.

Asadi and Khoshkhoo [15] evaluated the thermohydraulic performances on the water with various chevron angles. The results depicted that the optimal chevron angle was 60°. This was denoted by the highest heat transfer coefficient and the trend for the friction factor. As the chevron angle increases, so does the friction factor; however, at 60°, the results delineate an inverse relationship with the mass flow rate for both laminar and turbulent regimes. Kılıç and İpek [16] studied the heat transfer rate and overall effectiveness of corrugated plate heat exchangers experimentally. The chevron angles of interest were $\beta = 30°$ and $\beta = 60°$. As depicted by the results, the superior chevron angle was 60°. This is denoted by the higher heat transfer rate and overall effectiveness of the plate heat exchanger. Furthermore, the results also entailed that increasing the Reynolds number resulted in the heat transfer rate and overall effectiveness to augment; this was in agreement with previous studies.

Dolatabadi and Aghdam [17] presented the experimental and numerical analysis of the heat transfer and fluid flow of a triangular chevron plate heat exchanger. The studies were conducted with air as the working fluid with a uniform heat flux of 1350 W/m^2 applied to the wall. The Reynolds numbers, phase shifts, and channel heights varied in the ranges of $1000 < Re < 10{,}000$, $0° < \phi < 180°$, 5 mm < D < 35 mm, respectively. Increasing the Reynolds number decreased the fluid temperature significantly, leading to greater Nusselt numbers while simultaneously reducing the friction factor; this subsequently decreased the thermal efficiency factor. The Nusselt number for the chevron channels was higher than the plain channels due to increased turbulence intensities, leading to higher heat transfer rates. The best results obtained when accounting for the Nusselt number and friction factor, i.e., the thermal efficiency index, was at a phase difference of 90°. Lastly, the subsequential increase of distance between the surfaces (D) led to higher temperatures and lower Nusselt numbers/thermal efficiency factors. The volume of vortices causes this in the laminar sublayer, and the fluids' velocity decreases. As a result, to maximize the efficiency of the heat exchanger, the minimum distance between surfaces should be utilized.

Mohebbi and Veysi [18] investigated a small, brazed plate heat exchanger's thermohydraulic characteristics. The chevron angles were 60°, and the modified Wilson plot was incurred to calculate the Nusselt numbers. Chevron corrugations on plates were found to enhance the heat transfer and pressure drop. However, the results depict that the heat transfer and friction coefficients calculated in previous literature disagree up to 34% with

the results of this study in some cases. This implies that the correlations presented for large plate heat exchangers cannot be applied for small plate heat exchangers.

A numerical study on the thermohydraulic characteristics of water undergoing turbulent flow between two parallel chevron plates was presented by Jang and Lin [19]. The flow is incompressible, and the Chen κ-ε model was employed. The effects of three different chevron angles (20°, 40°, and 60°) relative to the direction of the main flow were investigated for inlet velocities ranging from 0.5 m/s–2.0 m/s. Increasing the chevron angle distorts streamlines, leading to stronger vortex zones. Hence, greater Nusselt numbers and pressure drops occur. Nusselt numbers were more significant near the wave bumps due to the wavy configurations interrupting the boundary layer. Lastly, higher inclination angles led to greater Colburn (j) and friction factors (f), with the inclination angle of 40° possessing the optimal goodness factor (j/f).

In the present paper, we investigate the performance of pin-fins in heat removal, forming a chevron shape structure. The novelty of this study is to investigate the presence of Chevron at different heights. Two critical parameters are studied in this analysis. The variable pin-fins height is implemented to investigate whether the higher the pin-fins, the better heat performance. The second is the replacement of the solid pin-fins with porous pin-fins with three different permeabilities of 10 PPI, 20 PPI, and 40 PPI, respectively. The porosity is constant and equal to 0.91 [20]. Section 2 presents the problem under investigation, followed by the finite element formulation in Section 3. Section 4 presents the results and discussion, and finally, the conclusion is in Section 5.

2. Problem Description

The model consists of an inlet and outlet cylinder connected to a mixing chamber. The testing chamber contains the pin-fins and is heated from below with a heated aluminum block, as shown in Figure 1. The entire model is made of aluminum, and the metal foams used in the pin-fins have three different permeabilities of 10 PPI, 20 PPI, and 40 PPI, respectively. Table 1 presents the properties of the aluminum metal foam used. The dimensions of the testing chamber are 37.5 mm by 37.5 mm and it has a height of 12.7 mm. The pin-fin heights vary between 2 mm, 4 mm, 6 mm, and 8 mm. The heated block is a square block with a similar base dimension to the test section with a thickness of 3.7 mm. The cylinder inlet and outlet diameter are set equal to 8 mm. The pin-fins have a cylindrical shape with a radius of 1 mm and variable lengths as indicated earlier of 2 mm, 4 mm, 6 mm, and 8 mm, respectively. As the flow enters the testing chamber, regardless of the pin-fin heights, some portion of the flow circulates between the pin-fins, and some will circulate above the pin-fins. This approach will reduce the pressure drop between the inlet and the outlet and, at the same time, will lead to a better heat enhancement. In our current study, distilled water maintained at 18 degrees Celsius is used as a circulating fluid. The physical properties of the water can be found in any textbook. Here, the Prandtl number of water is 6.83, its density is 998.2 kg/m^3, and its conductivity and viscosity are 0.613 W/m/K and 0.001002 kg/m/s, respectively. The heat flux is low so that the water maintains a single-phase flow.

Table 1. Properties of the Metallic aluminum Foam. Data from [20].

Foam Identification	Permeability κ(m^2)	Porosity ε
10 PPI	9.54788×10^{-7}	0.91
20 PPI	2.38697×10^{-7}	0.91
40 PPI	3.38×10^{-7}	0.91

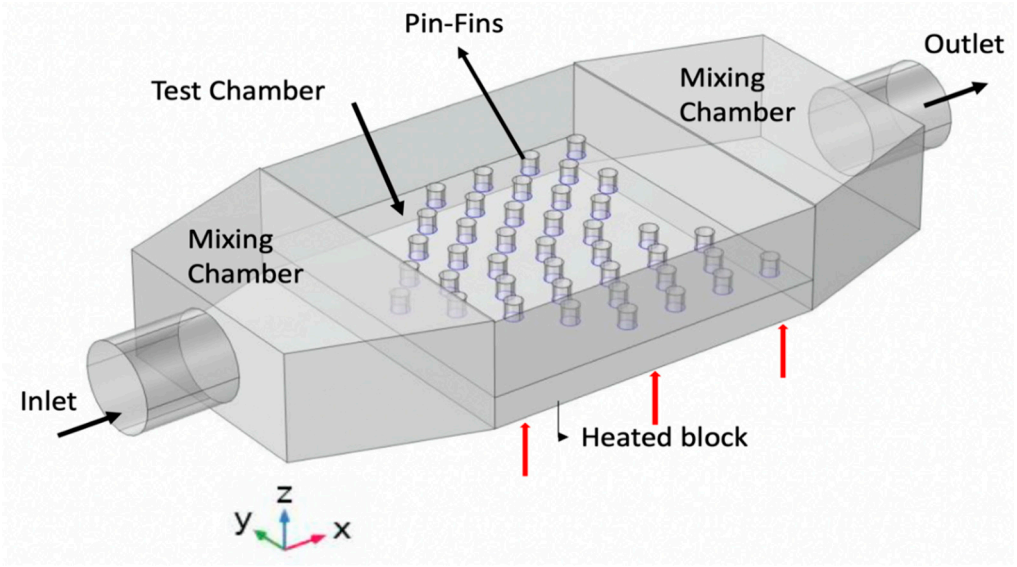

(**a**)

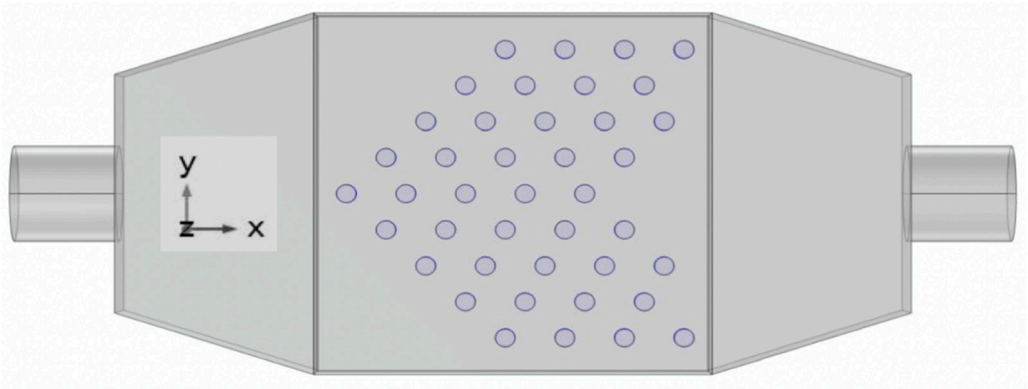

(**b**)

Figure 1. Model description: (**a**) 3D View; (**b**) Top View.

3. Finite Element Formulation

The full Navier–Stokes equation and the energy equation were solved numerically using the finite element method [20]. The set of a non-dimensional term used in our analysis are as follows:

$$U = \frac{u}{U_o}, V = \frac{v}{U_o}, W = \frac{w}{U_o} X = \frac{x}{De}, Y = \frac{y}{De}, Z = \frac{z}{De}, \theta = \frac{(T - T_{in})}{q''.\frac{De}{k_w}} \text{ and } P = \frac{pDe}{\mu U}, Da = \frac{\kappa}{De^2} \quad (1)$$

Here, De is the hydraulic diameter, k_w is the water conductivity, q" is the applied heat flux, T_{in} is the inlet temperature, and U_o is the inlet velocity. In particular, the momentum equations in the non-dimensional form are as follows in different directions:

Momentum equation along X-direction

$$Re\left(U\frac{\partial U}{\partial X} + V\frac{\partial U}{\partial Y} + W\frac{\partial U}{\partial Z}\right) = \frac{\partial P}{\partial X} + \left(\frac{\partial^2 U}{\partial X^2} + \frac{\partial^2 U}{\partial Y^2} + \frac{\partial^2 U}{\partial Z^2}\right) \quad (2)$$

Here, Re is the Reynolds number set equal to $Re = \frac{U_o De}{\nu}$.

Momentum equation along Y-direction

$$Re\left(U\frac{\partial V}{\partial X} + V\frac{\partial V}{\partial Y} + W\frac{\partial V}{\partial Z}\right) = \frac{\partial P}{\partial Y} + \left(\frac{\partial^2 V}{\partial X^2} + \frac{\partial^2 V}{\partial Y^2} + \frac{\partial^2 V}{\partial Z^2}\right) \quad (3)$$

Here, V is the velocity component in the Y direction.
Momentum equation along Z-direction

$$\mathrm{Re}\left(\mathrm{U}\frac{\partial \mathrm{W}}{\partial \mathrm{X}}+\mathrm{V}\frac{\partial \mathrm{W}}{\partial \mathrm{Y}}+\mathrm{W}\frac{\partial \mathrm{W}}{\partial \mathrm{Z}}\right)=\frac{\partial \mathrm{P}}{\partial \mathrm{Z}}+\left(\frac{\partial^2 \mathrm{W}}{\partial \mathrm{X}^2}+\frac{\partial^2 \mathrm{W}}{\partial \mathrm{Y}^2}+\frac{\partial^2 \mathrm{W}}{\partial \mathrm{Z}^2}\right) \tag{4}$$

Here, W is the velocity component in the Z direction.
Continuity equation
The continuity equation for this simulation can be expressed as

$$\left(\frac{\partial \mathrm{U}}{\partial \mathrm{X}}+\frac{\partial \mathrm{V}}{\partial \mathrm{Y}}+\frac{\partial \mathrm{W}}{\partial \mathrm{Z}}\right)=0 \tag{5}$$

Energy conservation equation
The energy equation is as follows:

$$\mathrm{RePr}\left(\mathrm{U}\frac{\partial \theta}{\partial \mathrm{X}}+\mathrm{V}\frac{\partial \theta}{\partial \mathrm{Y}}+\mathrm{W}\frac{\partial \theta}{\partial \mathrm{Z}}\right)=\left(\frac{\partial^2 \theta}{\partial \mathrm{X}^2}+\frac{\partial^2 \theta}{\partial \mathrm{Y}^2}+\frac{\partial^2 \theta}{\partial \mathrm{Z}^2}\right) \tag{6}$$

Here, θ is the non-dimensional temperature used in our calculation. The Prandtl number Pr is the ratio of the product of the specific heat of the fluid and the viscosity divided by the fluid conductivity. Thus, Pr is equal to $\frac{\mathrm{Cp}\mu}{\mathrm{k_w}}$.

3.1. Darcy–Brinkman Model

Since the flow rate within the system is low and the porosity of the metal foam is 0.91, the Darcy–Brinkman equations are used to analyze the fluid behavior. The equations in three dimensions are as follows:
Darcy–Brinkman in X direction

$$\frac{1}{\mathrm{Da}}\mathrm{U}=-\frac{\partial \mathrm{P}}{\partial \mathrm{X}}+\left(\frac{\partial^2 \mathrm{U}}{\partial \mathrm{X}^2}+\frac{\partial^2 \mathrm{U}}{\partial \mathrm{Y}^2}+\frac{\partial^2 \mathrm{U}}{\partial \mathrm{Z}^2}\right) \tag{7}$$

Here Da is the Darcy number known to be the ratio of the permeability to the square of the characteristic length.
Darcy–Brinkman in the Y *direction*

$$\frac{1}{\mathrm{Da}}\mathrm{V}=-\frac{\partial \mathrm{P}}{\partial \mathrm{Y}}+\left(\frac{\partial^2 \mathrm{V}}{\partial \mathrm{X}^2}+\frac{\partial^2 \mathrm{V}}{\partial \mathrm{Y}^2}+\frac{\partial^2 \mathrm{V}}{\partial \mathrm{Z}^2}\right) \tag{8}$$

Darcy–Brinkman in the Z direction

$$\frac{1}{\mathrm{Da}}\mathrm{W}=-\frac{\partial \mathrm{P}}{\partial \mathrm{Z}}+\left(\frac{\partial^2 \mathrm{W}}{\partial \mathrm{X}^2}+\frac{\partial^2 \mathrm{W}}{\partial \mathrm{Y}^2}+\frac{\partial^2 \mathrm{W}}{\partial \mathrm{Z}^2}\right) \tag{9}$$

The energy equation is written as follows:

$$\mathrm{RePr}\left(\mathrm{U}\frac{\partial \theta}{\partial \mathrm{X}}+\mathrm{V}\frac{\partial \theta}{\partial \mathrm{Y}}+\mathrm{W}\frac{\partial \theta}{\partial \mathrm{Z}}\right)=\left(\varphi+\frac{\mathrm{k_s}}{\mathrm{k_w}}(1-\varphi)\right)\left(\frac{\partial^2 \theta}{\partial \mathrm{X}^2}+\frac{\partial^2 \theta}{\partial \mathrm{Y}^2}+\frac{\partial^2 \theta}{\partial \mathrm{Z}^2}\right) \tag{10}$$

Here, φ is the porosity set equal to 0.91, and $\mathrm{k_s}$ is the conductivity of the solid porous material. It is important to mention that the conduction equation is used for the solid aluminum. The equation for the conduction heat transfer is shown in Equation (11) as follows:

$$k^*\left(\frac{\partial^2 \theta}{\partial \mathrm{X}^2}+\frac{\partial^2 \theta}{\partial \mathrm{Y}^2}+\frac{\partial^2 \theta}{\partial \mathrm{Z}^2}\right)=0 \tag{11}$$

Here, k^* is the ratio of the conductivity of the aluminum divided by the water conductivity. As the formulation is coupled, the equations were solved simultaneously using the finite element technique.

3.2. Boundary Conditions

At the inlet, the following boundary conditions are applied:

$$\theta = 0, U = 1 \tag{12}$$

At the outlet, the free boundary condition is applied; thus, the stress is set equal to zero. At the bottom of the plate, as shown in Figure 1a, the heat flux is set equal to 1. All other surfaces surrounding the model assume zero flux, thus being insulated.

3.3. Mesh Sensitivity Analysis

In order to use the optimum mesh size, mesh sensitivity tests were conducted for the five-chevron configuration. Table 2 presents the mesh size and the calculated average Nusselt number. Based on the data obtained in Table 2, the best mesh size is that of the normal mesh which consists of 692,064 elements. Furthermore, Figure 2 shows the mesh model used in the current analysis.

Table 2. Mesh analysis.

Mesh Size	Number of Elements	Average Nu Number	%Change
Extra coarse	57,996	8.32	-
Coarser	189,050	7.82	**6%**
Coarse	317,947	7.89	**0.88%**
Normal	692,064	7.85	**0.5%**

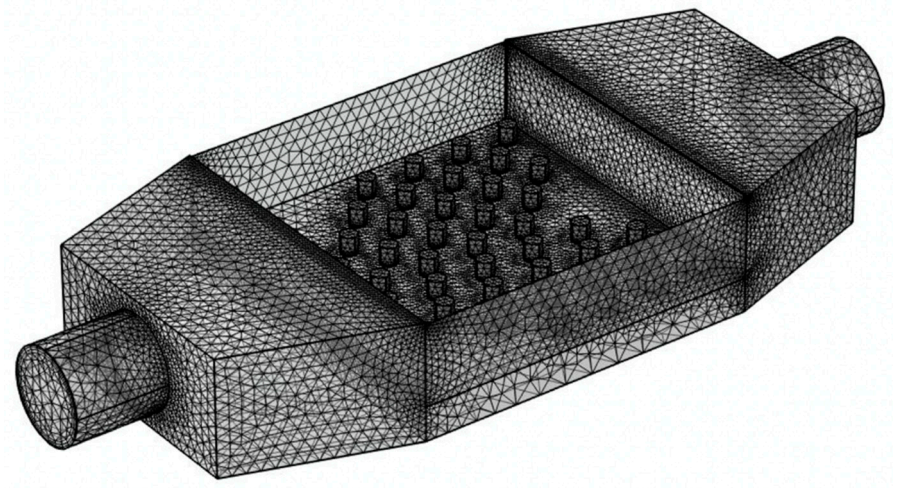

Figure 2. Mesh analysis.

3.4. Convergence Criteria

The numerical simulation was performed using the COMSOL Finite element software. At each iteration, the average relative error of the velocities, pressure, and temperature are each computed. These are obtained via the following relation:

$$R = \frac{1}{n.m} \sum_{i=1}^{i=m} \sum_{j=1}^{j=n} \left| \frac{\left(F_{i,j}^{s+1} - F_{i,j}^{s}\right)}{F_{i,j}^{s+1}} \right| \tag{13}$$

Here, F represents one of the unknowns, viz., U, V, W, P, or θ, and s is the iteration number, and (i, j) represents the coordinates on the grid. Convergence is reached if R for all the unknowns is below 1×10^{-6} in two successive iterations.

4. Validation of the Numerical Model

The numerical model is validated against an experimental measurement obtained by the author. Saghir et al. [21] studied heat enhancement in porous media. In the current paper, the insert consists of a chevron occupying a volume of 37.5 mm by 37.5 mm and with a height of 12.7 mm. In the experiment, this volume is replaced with porous media made of aluminum oxide with three different permeabilities of 10 PPI, 20 PPI, and 40 PPI. The porosity is constant and set equal to 0.91. All the boundary conditions and the heating condition in the current paper are identical to the experimental paper [21]. Three different heat fluxes were applied, and different inlet temperatures were measured. The temperature distribution was measured at a similar location to the present paper. Figure 3 shows the temperature distribution obtained experimentally and compared to the numerical model. The numerical results provided accurate calculations and were in good agreement with the experimental data. The fluid used in the model is a nanofluid which consists of 0.1% Al_2O_3 nanoparticles in distilled water. The flow rate is set equal to 0.1 US gallons per minute. The permeability, in this case, is 10 PPI. As the flow rate is low, the temperature magnitude increases, indicating less heat enhancement to the hot surface. Additionally, it is evident that as the heat fluxes increase, the temperature rises accordingly. The temperature variation is found to flatten due to the low flow rate.

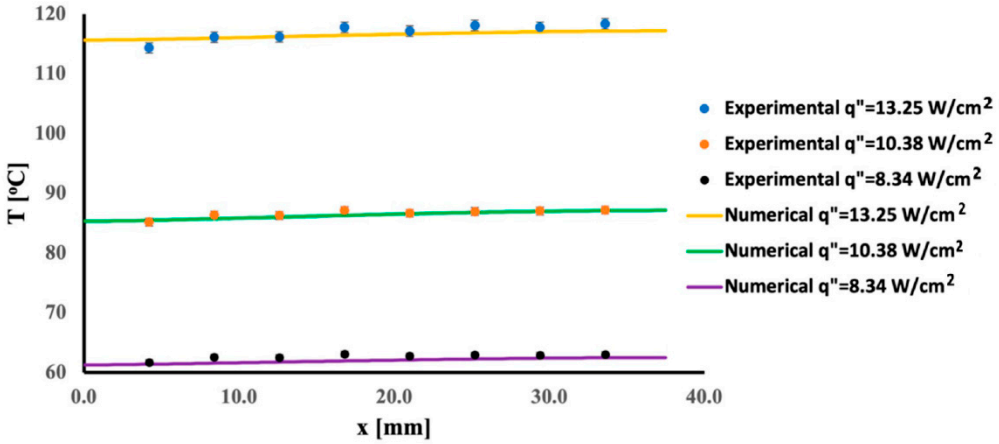

Figure 3. Temperature variation 1 mm below the interface.

5. Results and Discussion

The current paper focuses on investigating whether chevron pin-fins can achieve good heat removal from hot surfaces. In engineering, the pressure drop is a significant phenomenon that needs to be avoided to reduce the pumping power. Here two distributions of the chevron are investigated, with three chevrons occupying the test section and the five-chevron configuration. For each configuration, the chevron height varies from 2 mm to 8 mm with an increment of 2 mm. As the chevron reaches the height of 8 mm, the flow interaction between the chevrons and above them is minimum. The reason is that the total test section height is 12.7 mm and with 8 mm chevron adding the base height of 3.7 mm leaves very minimum space for the flow to circulate above the pin-fins. The first case with these configurations assumes the pin-fins are solid aluminum. In the second case, the chevron is porous; thus, flow can penetrate through the pin-fins, which may increase the heat extraction. The question which we need to address is whether porous pin-fins perform better than solid pin-fins.

5.1. Solid Pin-Fin Configurations

Based on the non-dimensional concept adopted in Equation (1), the Nusselt number is known to be the ratio of the convective heat transfer multiplied by the characteristic length of the fluid to the conductivity. Thus, $Nu = \frac{hDe}{k_w}$. However, since the convective heat coefficient "h" is known to be $h = \frac{q''}{(T-T_{in})}$, the Nusselt number becomes the inverse of the temperature in non-dimensional form. Thus, the local Nusselt number $Nu = \frac{1}{\theta}$. The temperature is calculated at the base of the pin-fins.

Figure 4 displays the average Nusselt number for the two-chevron configuration at different Reynolds numbers and different pin-fin heights. The flow rate represented by the Reynolds number varies from 50 to 900, while remaining in the laminar regime. The ascendant Nusselt variation as a function of the Reynolds number indicates the importance of the flow rate in extracting heat from the hot surface. This average Nusselt number is evaluated at the base of the pin-fins. It is evident that the highest pin-fins perform better in heat extraction and with the five-chevron configuration.

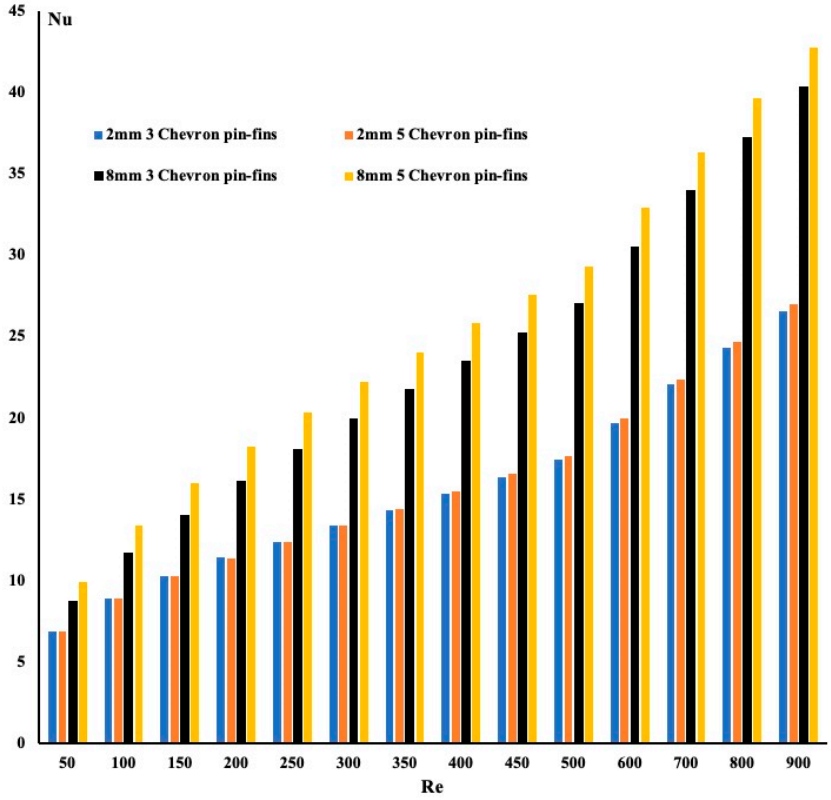

Figure 4. Nusselt number variation for solid pin-fins.

However, the large number of pin-fins in the flow path will increase the friction factor and create a more significant pressure drop. However, the pressure drop is not substantial because the flow circulates between the pin-fins and above them. The friction factor [20] in our case is defined as

$$f = 0.2529 \times \frac{\Delta P}{Re} \quad (14)$$

Here, $\frac{\Delta P}{Re}$ is the pressure drop ratio between the inlet and the outlet and the Reynolds number. The calculation results revealed that the highest pin-fins exhibit a more significant friction factor, and simultaneously, the friction factor f decreases as the Reynolds number increases. An additional observation is that the friction factor is identical for the two configurations when the pin-fins height is 2 mm. Based on the above statement and in order

to combine the flow effect and the heat effect in the model performance, the Performance Evaluation Criterion (PEC) is used and evaluated. In our study, it is defined as

$$\mathrm{PEC} = \frac{\mathrm{Nu}_{\mathrm{average}}}{\mathrm{f}^{1/3}} \tag{15}$$

Based on Equation (15), Figure 5 presents the Performance Evaluation criterion of the solid pin-fins for the two configurations and two pin-fin heights. As one may notice from Figure 5, the 2 mm pin-fins' height performance is identical whether one uses the three chevron configurations or the five chevron configurations. As the pin-fin height increases, the five-chevron configuration performs better than the three chevron configurations. The more significant number of pin-fins facilitates a more extensive heat extraction.

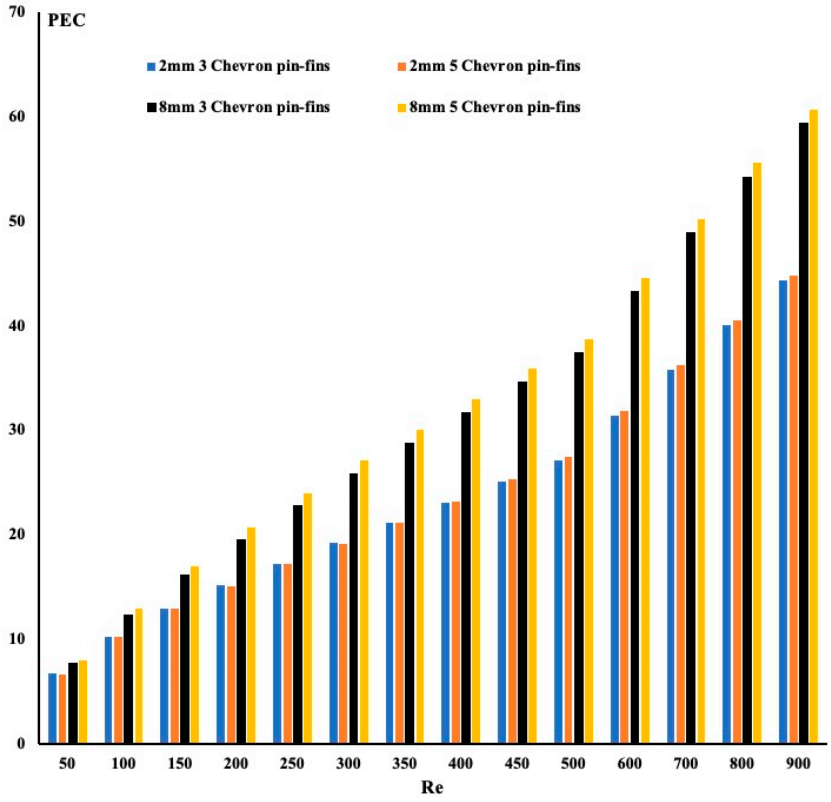

Figure 5. Performance evaluation criterion for solid pin-fins.

Finally, one way to determine the total amount of heat removed is by examining the temperature difference between the outlet and the inlet and multiplying this temperature by the fluid's heat capacity and the mass rate. In non-dimensional form, this formulation leads to

$$\text{Heat removed} = \mathrm{Pr} * \mathrm{Re} * \left(\theta_{\mathrm{out}} - \theta_{\mathrm{in}}\right) \tag{16}$$

As shown in Figure 6, the heat removed exhibits a nonlinear behavior as a function of the Reynolds number. This behavior is due to the fluid interaction between the portion flowing above and within the pin-fins. This mixing of fluid help extracts heat without affecting the pressure drop. One may conclude from this figure that the optimum pin-fin height for removing heat is when the pin-fin height is short, allowing the fluid mixing to occur. It is essential to indicate that this mixing is happening while in the laminar regime. One may summarize from this investigation that shorter pin-fins, by allowing mixing to happen, improve heat removal.

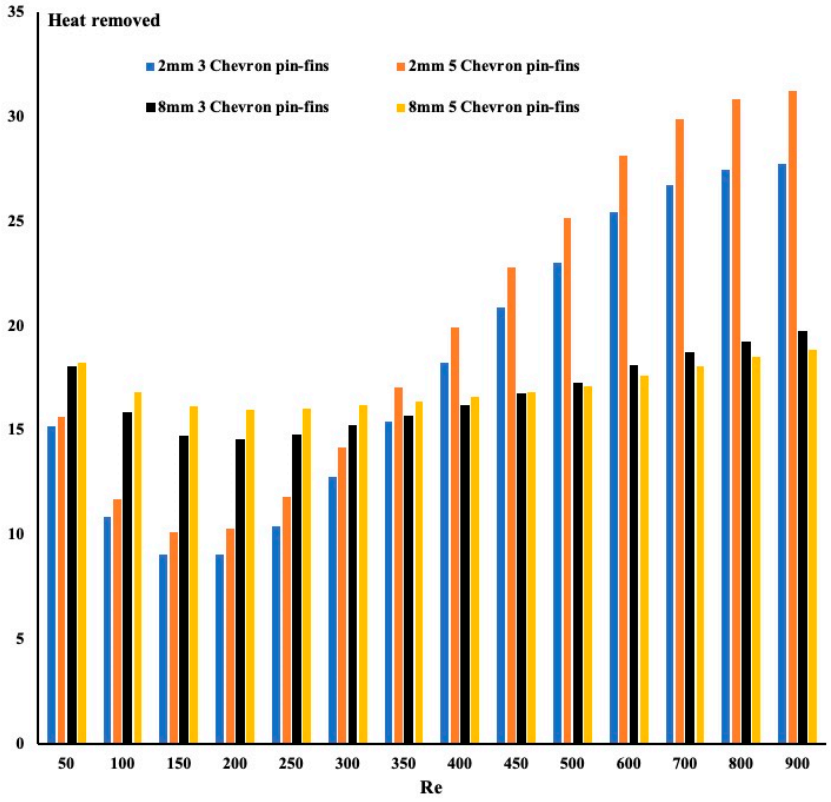

Figure 6. Heat removed using solid pin-fins.

5.2. Porous Pin-Fin Configuration

The previous investigation found that if the thermo-hydraulic problem is combined, the higher the pin-fins, the better performance is obtained. This is valid for any flow rate or for any Reynolds number on another term. The contact cross-section between the pin-fins and the heated plate remains constant during this investigation. In the present section, the pin-fins are rendered porous with three different permeability values of 10 PPI, 20 PPI, and 40 PPI. The porosity is maintained constant at 0.91. The uniqueness of this approach is that the flow will circulate between the pores of the pin-fins and around the pin-fins. One may expect a better heat transfer as the pore size increase. It is also interesting to verify whether the pressure drop will be less pronounced.

Figure 7 exhibits the variation of the average Nusselt number for all porous cases for two different porous pin-fin heights of 2 mm and 8 mm. As the pin-fin height increases, a nonlinear variation of the average Nusselt number is observed. This average Nusselt number profile was not observed with the solid pin-fin case. At a lower Reynolds number, the performance may appear attractive in some cases. Here again, the highest pin-fins provide the largest average Nusselt number. What is also interesting to observe is that with five chevron configurations, the average Nusselt number is more pronounced. Figure 8 presents the performance evaluation criterion for the 2 mm and 8 mm height, but maintains a permeability of 10 PPI to determine the effectiveness of using this type of configuration.

It is observed that the best configuration is a five-chevron configuration with a height of 8 mm. The reason for this variation is that it was found that the pressure drops, or in other words, the friction factor is close to identical for all cases under investigation for Reynolds numbers above 50. Thus, the change in the PEC is related to the average Nusselt number. The question would be, which configuration provides better heat removal? Figure 8 shows the heat removed for 10 PPI pin-fin cases and the two configurations under investigation.

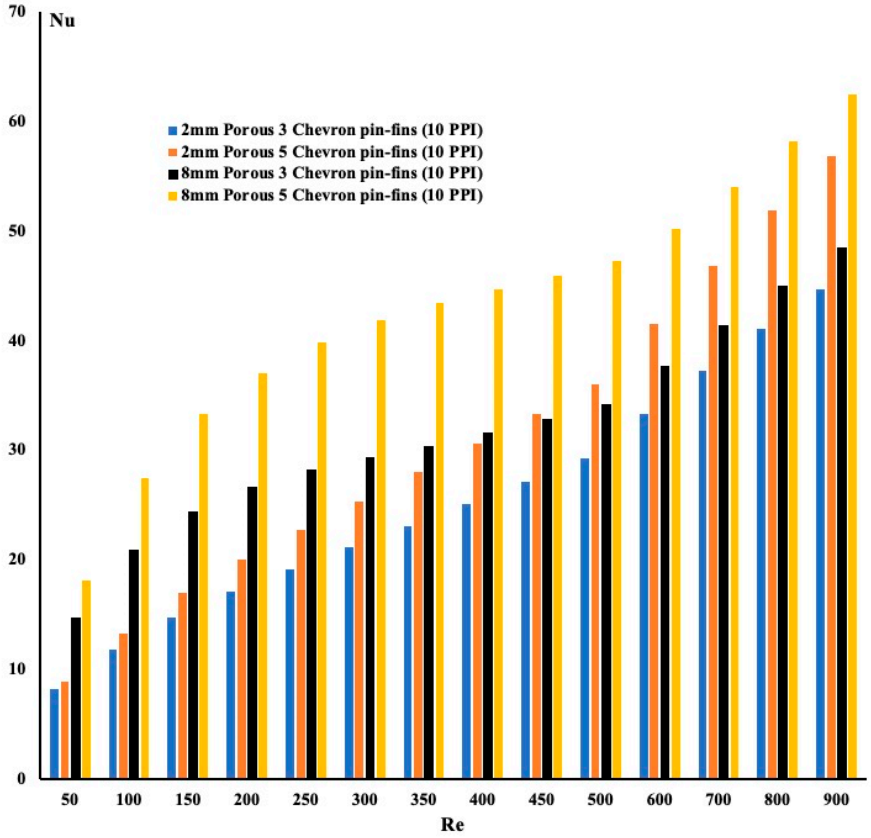

Figure 7. Average Nusselt number for porous pin-fins with a permeability of 10 PPI.

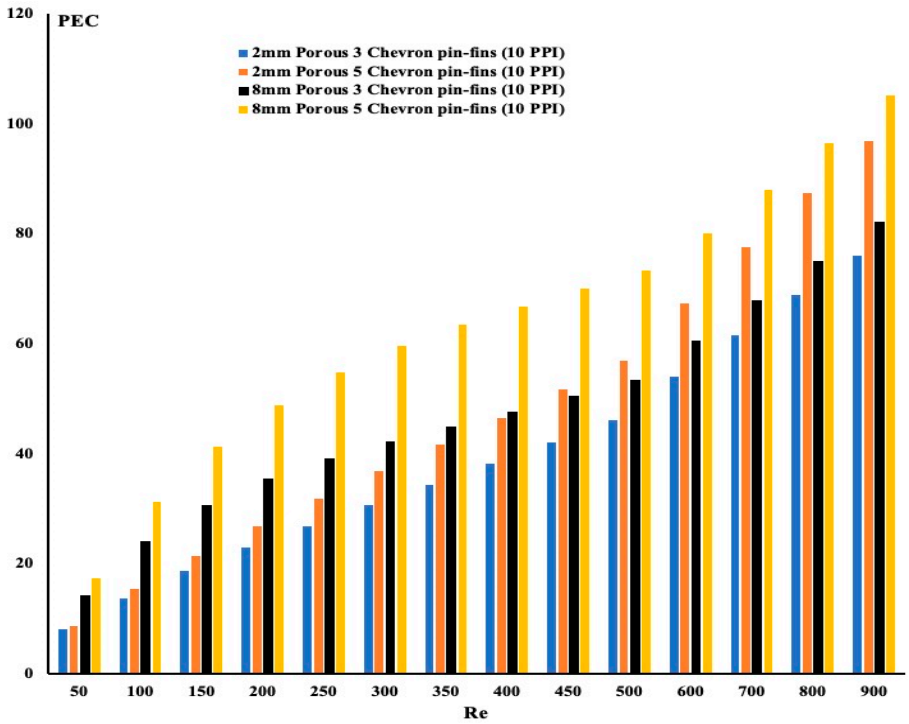

Figure 8. PEC for porous pin-fins with a permeability of 10 PPI.

It is interesting to observe, by examining Figure 9, that the porous pin-fins do not help in heat removal like the one obtained with solid pin-fins. In addition, the five-chevron configuration case outperforms the three-chevron configuration case. It appears that a

smaller volume of solid in the pin-fins leads us to believe that porous pin-fins may not be suitable for heat removal. Further investigation is needed which involves comparing all cases together.

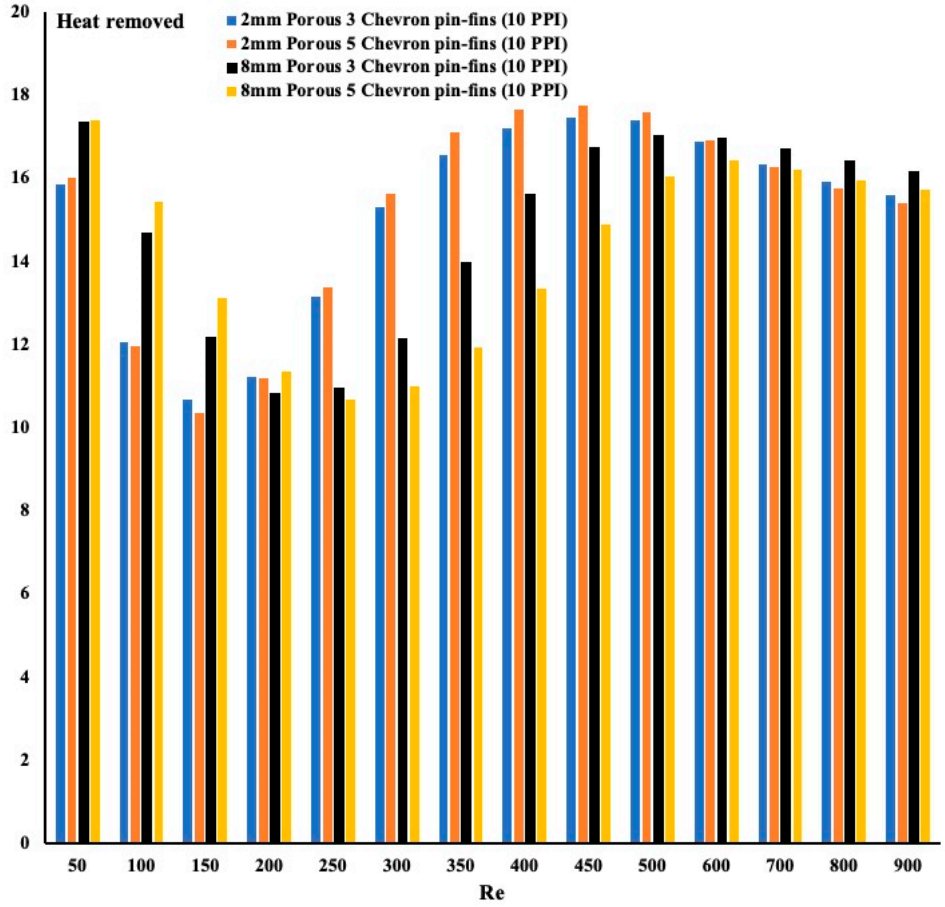

Figure 9. Heat removed using 10 PPI porous pin-fins.

5.3. Comparison of All Cases and Configurations

In the previous two sections, we demonstrated that the heat removed from the system is more significant when using solid pin-fins. Additionally, it was found that the higher the pin-fin height, the larger the average Nusselt number. A detailed comparison of all cases under investigation is presented to determine the best configuration for heat enhancement. The results are summarized for each pin-fin height separately.

Figure 10 presents the average Nusselt number for all pin-fin heights for the two configurations. Figure 10a displays the average Nusselt number when the pin-fins height is 2 mm. An increase in the Nusselt number as the Reynolds number increase is evident. It also appears that the porous pin-fins with a five-chevron configuration provide a larger Nusselt number. The solid pin-fin performance is the lowest of all cases. A linear variation of the average Nusselt number with the Reynolds number is obtained. Figure 10b shows similar cases when the pin-fin height is 4 mm. An increase in the average Nusselt number is noticeable. The five-chevron configuration with porous pin-fins continues to outperform the remaining cases. Amongst the porous pin-fins, the one with 10 PPI permeability is found to be the best. The nonlinear behavior of the Nusselt number for Re < 400 indicates that the linearity obtained previously disappeared due to flow mixing and boundary layer formation. As the pin-fins height increases to 6 mm, Figure 10c displays the average Nusselt number change with the Reynolds number. The Nusselt number magnitude increase further, and the porous pin-fins exhibit better performance than the other two cases. The variation of the Nusselt number remains the same as in the previous cases.

Finally, as the pin-fins' height increases to 8 mm (Figure 10d), the magnitude of the Nusselt number increases further, and the porous pin-fins outperform the other cases. We can summarize from Figure 10 that the porous pin-fins exhibit a more significant Nusselt number, and the longer the pin-fins, the greater the Nusselt number.

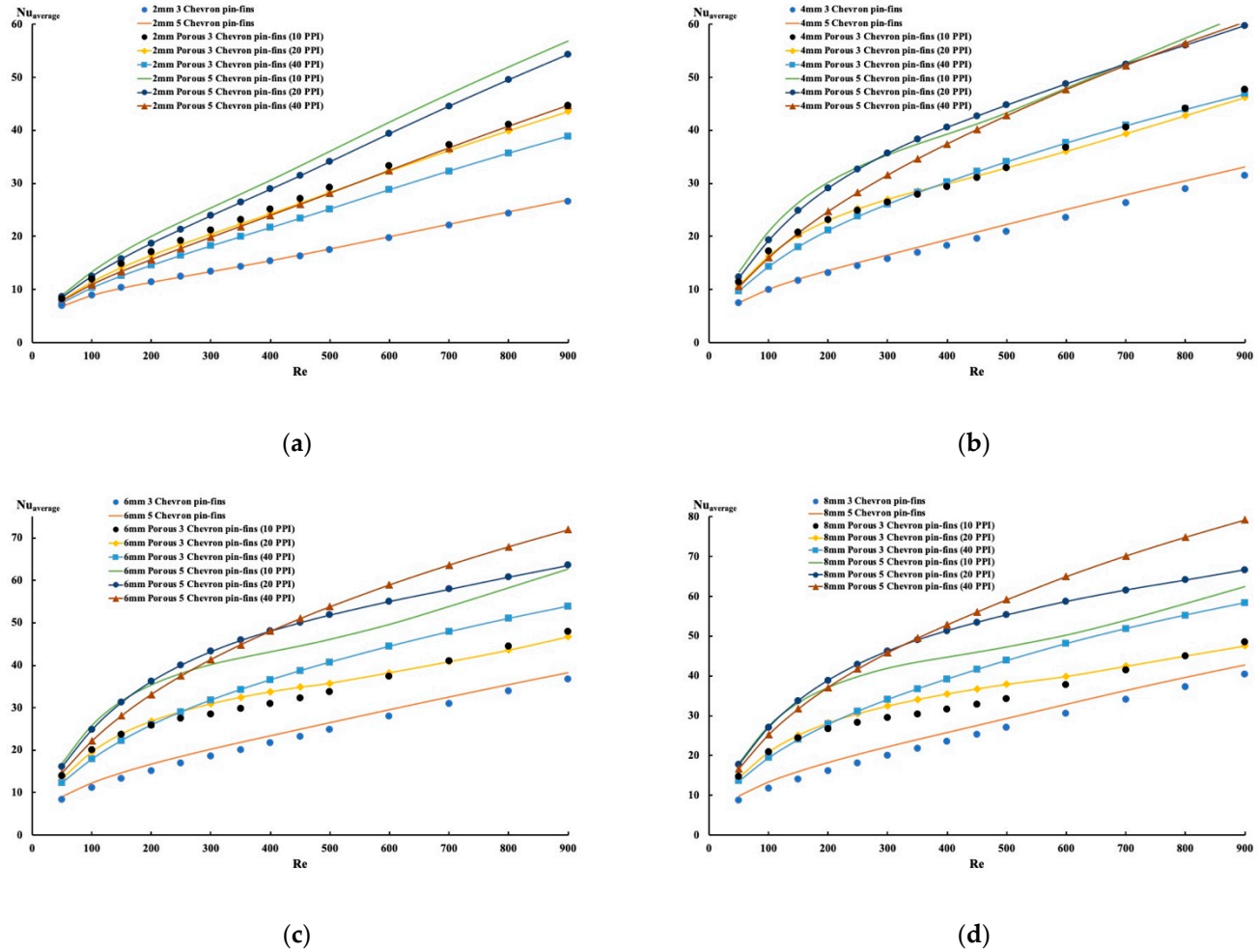

Figure 10. Average Nusselt variation for all cases: (**a**) 2 mm pin-fin height; (**b**) 4 mm pin-fin height; (**c**) 6 mm pin-fin height; (**d**) 8 mm pin-fin height.

When dealing with the flow around an obstacle like pin-fins, the system will have a friction effect which affects the pressure drop. Therefore, one way to combine the hydraulic effect with the heat effect is to investigate the performance evaluation criterion and assess the best configuration. Figure 11 shows the PEC for all cases and four different pin-fins heights. Figure 11a displays the cases for a pin-fin height of 2 mm. As the height is minimal, it was found that the friction coefficient is identical for all cases, with an increase in magnitude for a low Reynolds number. As the Reynolds number increase, the friction factor decreases. Thus, the variation of PEC for this case, as displayed in Figure 11a, is identical to the average Nusselt number variation displayed in Figure 10a. As the pin-fin height reaches 4 mm, as shown in Figure 10b, the magnitude of PEC increases further, and the five-chevron configuration of porous pin-fins outperforms the other cases.

Furthermore, Figure 10c presents the case when the pin-fins height is 6 mm in this study. Similar behavior as previously with greater PEC magnitude is displayed, and, finally, Figure 11d corresponds to pin-fin heights of 8 mm. What is interesting to learn from this figure is that the thermohydraulic performance of pin-fins is more pronounced with porous pin-fins and increases as the pin-fins height increase. Another interesting finding is that

permeability plays a role in thermohydraulic performance. The flow circulation inside the pin-fins is critical to improving heat extraction.

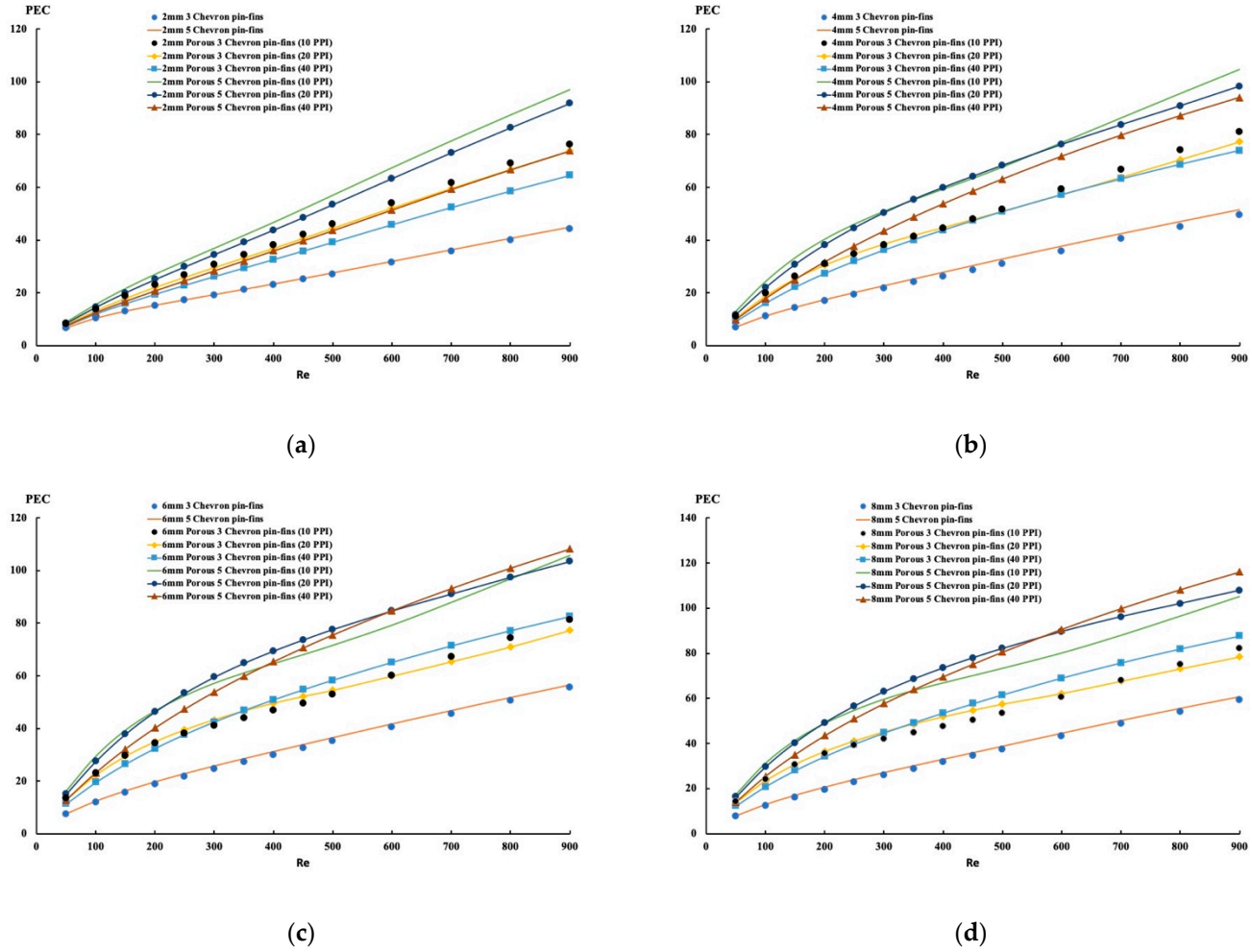

Figure 11. PEC variation for all cases: (**a**) 2 mm pin-fin height; (**b**) 4 mm pin-fin height; (**c**) 6 mm pin-fin height; (**d**) 8 mm pin-fin height.

It is interesting to examine the amount of heat absorbed by the water and determine the best configuration. Based on Equation (15), the amount of heat absorbed is a function of the outlet temperature and the Reynolds and Prandtl numbers. Figure 12 presents the heat removed as a function of the Reynolds number for all cases. Figure 12a shows the heat released for the 2 mm pin-fin height. A nonlinear variation is noticeable, with the lowest heat removed having a Reynolds number of approximately 200. As the Reynolds number increase beyond 200, the mixing mechanism created by the presence of pin-fins increases the heat absorbed by the fluid.

Interestingly, the solid pin-fins with a five-chevron configuration exhibit the highest heat removed, followed by the porous five-chevron-configuration pin-fins with a permeability of 40 PPI. The structure of the 40 PPI pin-fins is closer to solid pin-fins, hence the similar performance. As the permeability increases, the water absorbs less heat. With an increase in pin-fin height to 4 mm, Figure 11b presents the heat removed profile for all cases. The minimum heat removed around a Reynolds number of 200 is identical to the previous case, and the solid pin-fins and the porous pin-fins with low permeability remain the best choices. Figure 12c,d presents the heat removed for the two remaining pin-fin heights of 6 mm and 8 mm, respectively.

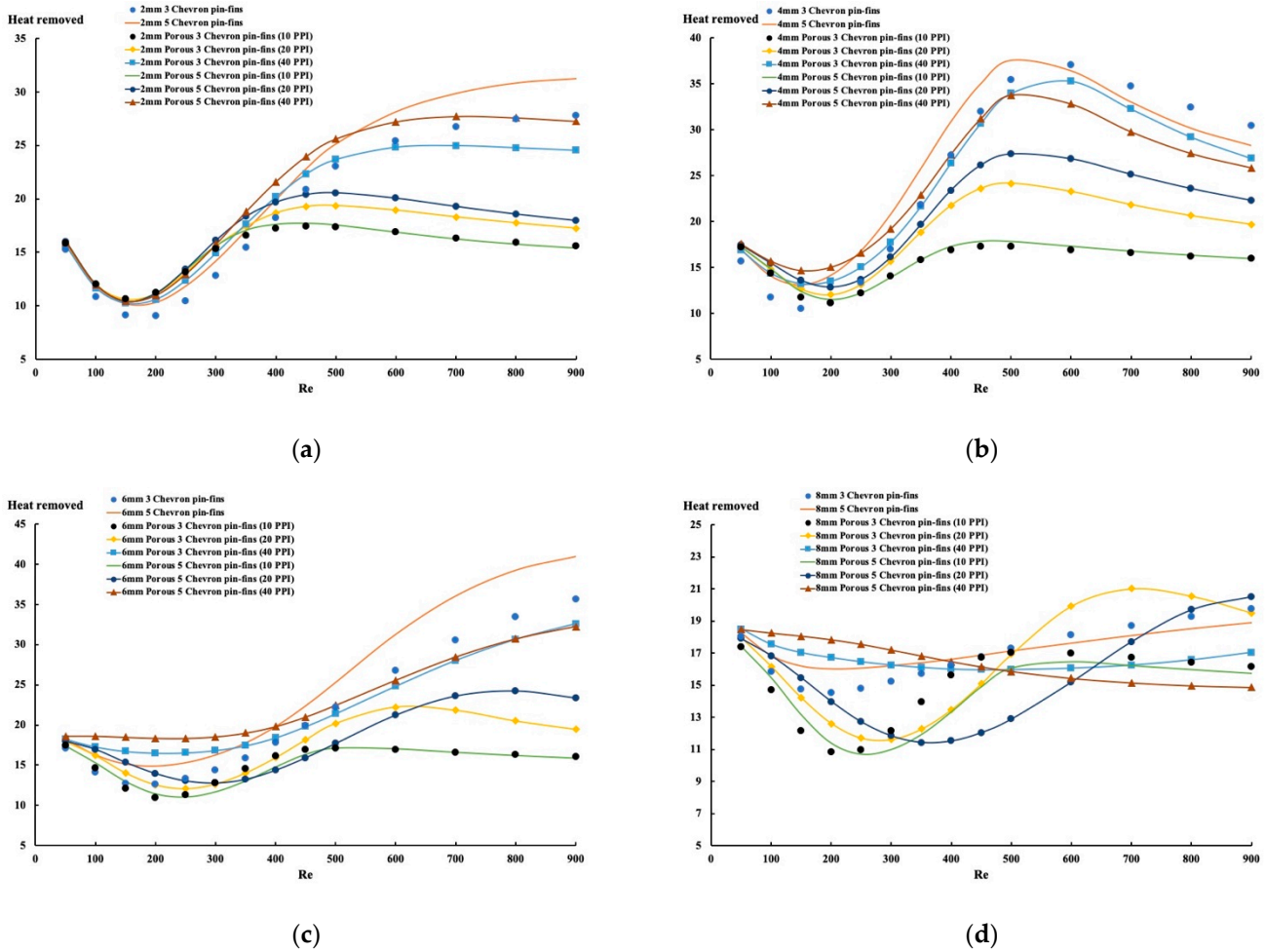

Figure 12. Heat-removed variation for all cases: (**a**) 2 mm pin-fin height; (**b**) 4 mm pin-fin height; (**c**) 6 mm pin-fin height; (**d**) 8 mm pin-fin height.

Interestingly, as the pin-fin height reaches a maximum of 8 mm, heat removed from the system behaves differently for each case. For some cases, a minimum increase of heat was released as the Reynolds number increases, and the amount of heat absorbed by the water for all cases at 8 mm pin-fins is the lowest compared to other pin-fin heights. This indicates that the PEC for 8 mm is found to be the best, but at the expense of high pumping power. Finally, Figure 13 presents a cross-section view of the typical temperature distribution along the flow path. It is evident the flow removes the heat from the hot surface toward the water exit. This is shown for the shortest pin-fins.

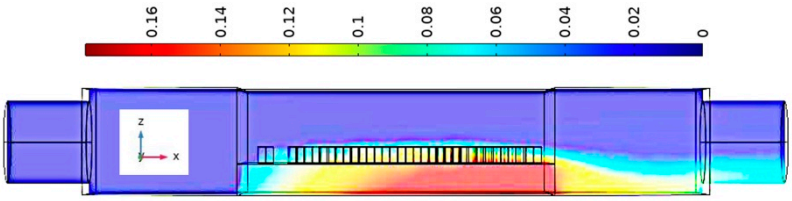

Figure 13. Temperature distribution along the flow path at mid-section.

6. Conclusions

The present study examines heat enhancement in a pin-fin-forming chevron configuration. Two types of pin-fins were studied. The first features cylindrical solid aluminum, and the second one is porous aluminum. Three different permeabilities of 10 PPI, 20 PPI,

and 40 PPI for the porous pin-fins were investigated by maintaining a constant porosity of 0.91. Three chevrons and five chevrons' configurations were studied. The complete Navier–Stokes equation, continuity equation, and the energy equation were solved numerically. For the porous case, the Darcy–Brinkman model was used. Four different pin-fins heights of 2 mm, 4 mm, 6 mm, and 8 mm were used in this study. The results reveal the following:

1. As the pin-fins height increases, the Nusselt number increases with the Reynolds number. The largest average Nusselt number was obtained for 8 mm porous pin-fin height;
2. The friction coefficient is identical for all cases when the pin-fin heights are at their lowest level of 2 mm. As the pin-fins height increase, the solid pin-fins exhibit a more significant friction factor when compared to the porous pin-fins;
3. By combining the average Nusselt number with the friction coefficient, the performance evaluation criterion (PEC) is higher as the pin-fins height increases, and the porous pin-fins exhibit the greater PEC amongst all cases regardless of the pin-fins' height;
4. If one ignores the friction and pressure drop effect, it is found that the fluid absorbed more heat when the pin-fins height was at 4 mm in height. The porous pin-fins delivered less heat to the fluid when compared to the solid pin-fins.

Author Contributions: Conceptualization, M.Z.S. and I.G.; methodology, M.Z.S.; software, M.Z.S.; validation, M.Z.S.; formal analysis, M.Z.S.; investigation, M.Z.S.; resources, I.G.; data curation, M.Z.S.; writing—original draft preparation, M.Z.S. All authors have read and agreed to the published version of the manuscript.

Funding: This research is funded by National Science and Engineering Research Canada (NSERC).

Conflicts of Interest: The authors declare no conflict of interest.

References

1. Martin, H. A theoretical approach to predict the performance of chevron-type plate heat exchangers. *Chem. Eng. Processing Process Intensif.* **1996**, *35*, 301–310. [CrossRef]
2. Dović, D.; Palm, B.; Švaić, S. Generalized correlations for predicting heat transfer and pressure drop in plate heat exchanger channels of arbitrary geometry. *Int. J. Heat Mass Transf.* **2009**, *52*, 4553–4563. [CrossRef]
3. Huang, D.; Wu, Z.; Sunden, B. Pressure drop and convective heat transfer of Al_2O_3/water and MWCNT/water nanofluids in a chevron plate heat exchanger. *Int. J. Heat Mass Transf.* **2015**, *89*, 620–626. [CrossRef]
4. Al-Neama, A.F.; Khatir, Z.; Kapur, N.; Summers, J.; Thompson, H.M. An experimental and numerical investigation of chevron fin structures in serpentine minichannel heat sinks. *Int. J. Heat Mass Transf.* **2018**, *120*, 1213–1228. [CrossRef]
5. Zhu, X.; Haglind, F. Relationship between inclination angle and friction factor of chevron-type plate heat exchangers. *Int. J. Heat Mass Transf.* **2020**, *162*, 120370. [CrossRef]
6. Fernandes, C.S.; Dias, R.P.; Nóbrega, J.M.; Maia, J.M. Laminar flow in chevron-type plate heat exchangers: CFD analysis of tortuosity, shape factor and friction factor. *Chem. Eng. Processing Process Intensif.* **2007**, *46*, 825–833. [CrossRef]
7. Tsai, Y.C.; Liu, F.B.; Shen, P.T. Investigations of the pressure drop and flow distribution in a chevron-type plate heat exchanger. *Int. Commun. Heat Mass Transf.* **2009**, *36*, 574–578. [CrossRef]
8. Han, X.H.; Cui, L.Q.; Chen, S.J.; Chen, G.M.; Wang, Q. A numerical and experimental study of chevron, corrugated-plate heat exchangers. *Int. Commun. Heat Mass Transf.* **2010**, *37*, 1008–1014. [CrossRef]
9. Kumar, B.; Soni, A.; Singh, S.N. Effect of geometrical parameters on the performance of chevron type plate heat exchanger. *Exp. Therm. Fluid Sci.* **2018**, *91*, 126–133. [CrossRef]
10. Kumar, B.; Singh, S.N. Analytical studies on the hydraulic performance of chevron type plate heat exchanger. *Int. J. Heat Technol.* **2015**, *33*, 17–24. [CrossRef]
11. Naik, V.R.; Matawala, V.K. Experimental investigation of single phase chevron type gasket plate heat exchanger. *Stainl. Steel* **2013**, *316*, 16–25.
12. Jain, S.; Joshi, A.; Bansal, P.K. A new approach to numerical simulation of small-sized plate heat exchangers with chevron plates. *J. Heat Transf.* **2007**, *129*, 291–297. [CrossRef]
13. Muley, A.; Manglik, R.M. Experimental study of turbulent flow heat transfer and pressure drop in a plate heat exchanger with chevron plates. *Trans. ASME J. Heat Transf.* **1999**, *121*, 110–117. [CrossRef]
14. Muley, A.; Manglik, R.M.; Metwally, H.M. Enhanced heat transfer characteristics of viscous liquid flows in a chevron plate heat exchanger. *J. Heat Transf.* **1999**, *121*, 1011–1017. [CrossRef]

15. Asadi, M.; Khoshkhoo, R.H. Effects of chevron angle on thermal performance of corrugated plate heat exchanger. *Int. J. Eng. Pract. Res.* **2014**, *3*, 8. [CrossRef]
16. Kılıç, B.; İpek, O. Experimental investigation of heat transfer and effectiveness in corrugated plate heat exchangers having different chevron angles. *Heat Mass Transf.* **2017**, *53*, 725–731. [CrossRef]
17. Dolatabadi, H.; Aghdam, A.H. Experimental and numerical study of the heat transfer and pressure drop in triangular chevron channels. *J. Theor. Appl. Mech.* **2018**, *56*, 751–763. [CrossRef]
18. Mohebbi, S.; Veysi, F. An experimental investigation on the heat transfer and friction coefficients of a small plate heat exchanger with chevron angle. *Heat Mass Transfer* **2020**, *56*, 849–858. [CrossRef]
19. Jang, J.Y.; Chien-Nan, L. A numerical analysis of three-dimensional heat transfer and fluid flow in Chevron plate channels/Discussion. *ASHRAE Trans.* **2000**, *106*, 856.
20. Bayomy, A.M.; Saghir, M.Z. Heat transfer characteristics of aluminum metal foam subjected to a pulsating/steady water flow: Experimental and numerical approach. *Int. J. Heat Mass Transf.* **2016**, *97*, 318–333. [CrossRef]
21. Saghir, M.Z.; Welsford, C.; Thanapathy, P.; Bayomy, A.M.; Delisle, C. Experimental measurements and Numerical computation of nano heat transfer enhancement inside a porous material. *J. Therm. Sci. Eng. Appl.* **2020**, *12*, 011003. [CrossRef]